Cite as: W. Lu *et al.*, *Science* 10.1126/science.aar5372 (2018).

Late inception of a resiliently oxygenated upper ocean

Wanyi Lu,[1] Andy Ridgwell,[2,3] Ellen Thomas,[4,5] Dalton S. Hardisty,[6] Genming Luo,[7] Thomas J. Algeo,[7,8,9] Matthew R. Saltzman,[10] Benjamin C. Gill,[11] Yanan Shen,[12] Hong-Fei Ling,[13] Cole T. Edwards,[14] Michael T. Whalen,[15] Xiaoli Zhou,[1] Kristina M. Gutchess,[1] Li Jin,[16] Rosalind E. M. Rickaby,[17] Hugh C. Jenkyns,[17] Timothy W. Lyons,[2] Timothy M. Lenton,[18] Lee R. Kump,[19] Zunli Lu[1]*

[1]Department of Earth Sciences, Syracuse University, Syracuse, NY, USA. [2]Department of Earth Sciences, University of California, Riverside, Riverside, CA, USA. [3]School of Geographical Sciences, University of Bristol, Bristol, UK. [4]Department of Geology and Geophysics, Yale University, New Haven, CT, USA. [5]Department of Earth and Environmental Sciences, Wesleyan University, Middletown, CT, USA. [6]Department of Earth and Environmental Sciences, Michigan State University, East Lansing, MI, USA. [7]State Key Laboratory of Biogeology and Environmental Geology and School of Earth Science, China University of Geosciences, Wuhan, China. [8]State Key Laboratory of Geological Processes and Mineral Resources, China University of Geosciences, Wuhan, China. [9]Department of Geology, University of Cincinnati, Cincinnati, OH, USA. [10]School of Earth Sciences, The Ohio State University, Columbus, OH, USA. [11]Department of Geosciences, Virginia Polytechnic and State University, Blacksburg, VA, USA. [12]School of Earth and Space Sciences, University of Science and Technology of China, Hefei, China. [13]State Key Laboratory for Mineral Deposits Research, School of Earth Sciences and Engineering, Nanjing University, Nanjing, China. [14]Department of Geological and Environmental Sciences, Appalachian State University, Boone, NC, USA. [15]Department of Geosciences, University of Alaska, Fairbanks, Fairbanks, AK, USA. [16]Geology Department, State University of New York College at Cortland, Cortland, NY, USA. [17]Department of Earth Sciences, University of Oxford, Oxford, UK. [18]Earth System Science group, College of Life and Environmental Sciences, University of Exeter, Exeter, UK. [19]Department of Geosciences, Pennsylvania State University, University Park, PA, USA.

***Corresponding author. Email: zunlilu@syr.edu**

Rising oceanic and atmospheric oxygen levels through time have been crucial to enhanced habitability of surface Earth environments. Few redox proxies can track secular variations in dissolved oxygen concentrations ([O_2]) around threshold levels for metazoan survival in the upper ocean. We present an extensive compilation of iodine to calcium ratios (I/Ca) in marine carbonates. Our record supports a major rise in atmospheric pO_2 at ~400 million years ago (Ma), and reveals a step-change in the oxygenation of the upper ocean to relatively sustainable near-modern conditions at ~200 Ma. An Earth system model demonstrates that a shift in organic matter remineralization to greater depths, which may have been due to increasing size and biomineralization of eukaryotic plankton, likely drove the I/Ca signals at ~200 Ma.

The evolution and survival of marine animals depends on oxygen availability, particularly in upper ocean waters – ranging from the sea surface to the thermocline – during early Earth history (*1*). The [O_2] in the upper ocean commonly decreases from the well-mixed surface ocean (top few tens of meters) into deeper subsurface waters (a few hundred meters). This [O_2] gradient is controlled by three key factors: (i) the partial pressure of oxygen in the atmosphere (pO_2), (ii) the intensity of upper ocean mixing and (iii) oxidation of organic matter in the water column which consumes oxygen (*2*). Atmospheric pO_2 changes through time have been estimated via geochemical proxy data and box models (*3*). Oceanic paleo-redox proxies typically track the areal extent of euxinic waters (containing H_2S) and the presence/absence of anoxia (positive/zero [O_2]) (*4*, *5*). Since most modern marine animals are sensitive to [O_2] changes between ~10 and ~100 μmol/kg (*2*), development of long-term proxy reconstructions for [O_2] in this critical range (oxic–hypoxic) would help elucidate when and how oceanic oxygenation evolved to accommodate the modern ecological landscape.

Carbonate I/Ca is one of the novel proxies developed for the oxic–hypoxic window with the potential to reconstruct secular trends in upper-ocean oxygenation (*6*, *7*). The long residence time of iodine (~300 kyr) leads to generally uniform total iodine concentrations in the modern ocean, but speciation changes of iodine between iodate (IO_3^-) and iodide (I^-) are controlled locally (*8*, *9*). IO_3^- is completely reduced to I^- in waters at low [O_2] (*8*, *9*) and re-oxidized under well-oxygenated conditions. Since IO_3^- is the only chemical form of iodine incorporated into the carbonate structure (*7*) by replacing the CO_3^{2-} ion (*10*), carbonate I/Ca records of local seawater [IO_3^-] through time can indicate changes in [O_2]. Carbonate I/Ca has been shown to be a reliable tracer responding primarily to [O_2] variations in marine environments over a wide range of geological periods (*6*, *11*–*16*).

We measured I/Ca in an extensive Phanerozoic collection of shallow marine carbonates likely forming within the top 200 m of the water column and compiled them with published data (table S1 and Fig. 1A). Maximum I/Ca values for individual localities were generally low in the Proterozoic, except for periods which have been associated with potential atmospheric pO_2 rises [e.g., the Great Oxidation Event (*12*) and some Neoproterozoic carbon isotope excursions (*11*, *15*), when maximum values temporarily increased to Cenozoic levels (3–4 μmol/mol) (Fig. 1A). Paleozoic maximum values are comparable to those of the Proterozoic, despite a rela-

tively short spike during the Devonian, at approximately 400 Ma, when the 75th percentile values reached Cenozoic levels. Break point analyses indicate a step-change at Triassic to early Jurassic (~200 Ma, fig. S1), after which maximum values remain above 4 μmol/mol and 75th percentile values are mostly higher than 3 μmol/mol (*6*, *13*). The Devonian I/Ca excursion and the step-change at ~ 200 Ma are two key observations in this data compilation.

The stark contrast between predominantly low Paleozoic values and high Meso-Cenozoic values (excluding the Triassic, i.e., <200 Ma) cannot be explained by sampling biases. The sample size for the Paleozoic (n = 894) is comparable to that for the Proterozoic (n = 1078) and the Meso-Cenozoic (n = 926). The sampling density (number of samples per unit time) is similar in the Paleozoic and Meso-Cenozoic, although lower in the Proterozoic (Fig. 1B). For Paleozoic samples, we targeted carbonate- and fossil-rich (shallow) continental-shelf locations, i.e., relatively well-oxygenated settings, which are prone to record high I/Ca values. By contrast, many Mesozoic data were generated from sections recording well-established global oceanic anoxic events (OAEs), which, if anything, would bias that dataset toward low values. Cenozoic I/Ca values were measured in sediment coarse fraction, which may better preserve primary I/Ca signatures than bulk-rock samples. Existing early Cenozoic (*14*) and Cretaceous I/Ca data (*13*) are generally comparable across different lithologies, although comparisons between the Cenozoic and other periods are more tenuous. The current data set has relatively denser sample coverage for intervals coinciding with Earth-system perturbations (e.g., major carbon-isotope excursions and mass extinctions) than for extended intervals with limited environmental changes, but this should not influence main features of the data compilation.

I/Ca values can potentially be reduced during subaerial exposure, marine burial and dolomitization, but no post-depositional alterations are known to increase I/Ca (*11*). A variety of diagenesis indicators were considered in previous studies of samples that we used here (*7*, *15–17*). In all of those case studies, the number of potentially altered samples was limited and did not influence the central trend of the majority of the data through time, as represented by the 25th and 75th percentile values (Fig. 1A). High I/Ca values throughout the record (Fig. 1A) are not consistently tied to a specific inferred primary carbonate mineralogy (e.g., calcite *vs* aragonite seas, fig. S2A). The distinct behaviors of I/Ca before and after ~200 Ma (Fig. 1A) cannot be explained by secular changes in seawater [Ca^{2+}] (fig. S2B). No evidence suggests that differences in Paleozoic and Mesozoic I/Ca distributions were due to uniformly greater alteration of the Paleozoic samples (fig. S3). Lower relative standard deviations (RSD) of neighboring samples in each section (i.e., smoother I/Ca profiles; fig. S4) may reflect better preservation of the Paleozoic than the Proterozoic samples (fig. S4).

We interpret I/Ca in marine carbonates primarily as a qualitative indicator for the depth of the oxycline (Fig. 2), i.e., that part of water column where the [O_2] decreases relatively abruptly. Carbonate rocks formed in the upper ocean record surface or near-surface seawater [IO_3^-], which is strongly affected by the presence/absence of a proximal oxygen minimum zone (OMZ) or a shallow oxycline. Due to the relatively slow oxidation kinetics of I^- (*18*), surface waters may retain a low iodate signal despite high in situ [O_2] levels. For instance, core-top (modern) planktonic foraminiferal shells exhibit low I/Ca values (~0.5 μmol/mol) in waters above a shallow OMZ in the equatorial Pacific, but record higher values (>3 μmol/mol) at other well-oxygenated locations (*6*).

The large I/Ca excursion during the Devonian (Fig. 3) most likely reflects deepening of the oxycline and development of better oxygenated conditions in the upper ocean, consistent with published proxy data and modeling results (*4*, *5*, *19*, *20*). Although different box models yield somewhat divergent interpretations of atmospheric pO_2 variation through the Phanerozoic (*21–24*), a Devonian rise in pO_2 levels is plausible, based on the COPSE model and charcoal proxy reconstructions (Fig. 3A), and was most likely due to increased abundance of vascular land plants (*19*, *20*). Previous work interpreted δ^{98}Mo, iron-speciation and biological data (Fig. 3C) to reflect oceanic redox changes, supporting the idea of atmospheric pO_2 rise during the Devonian (*4*, *5*). The combination of these independent proxies indicates that the Devonian atmospheric pO_2 rise impacted the whole atmosphere-ocean system, across the entire redox spectrum (Fig. 3).

I/Ca values returned to Proterozoic-like levels following the transient Devonian excursion, but there is no evidence for a pO_2 decrease to pre-Devonian levels between the Carboniferous and the Triassic. Instead, the post-Devonian atmosphere was probably relatively O_2-rich (Fig. 3A). High atmospheric pO_2 likely altered terrestrial weathering feedbacks and enhanced nutrient delivery to the ocean (*25*, *26*), leading to intensified O_2 consumption in the upper ocean, a generally shallow oxycline, and low I/Ca values between ~400 and 200 Ma (Fig. 3B). Under such conditions, carbonates formed in surface-oceans rapidly equilibrated with the high-pO_2 atmosphere would record low in situ [IO_3^-] due to the slow oxidation of I^- during mixing between surface and subsurface waters (Fig. 2B). If the oxycline were indeed shallow, marine animals on continental shelves at that time (~ 200-400 Ma) would have been living in a thin layer of well-oxygenated surface water directly underlain by an OMZ (Fig. 2B). Our dataset (Fig. 1A) implies that well-oxygenated upper-ocean conditions became persistent and resilient only by the Triassic-Jurassic (~200 Ma), much later than previously in-

ferred (*27*). The prerequisites for achieving such well-oxygenated upper-ocean conditions are a combination of high atmospheric pO_2 and a generally deep oxycline (Fig. 2C). The position of the oxycline is strongly controlled by the depth of organic-matter remineralization, which is dependent on the efficiency of organic-matter export from the photic zone, and has been proposed as a governing parameter for OMZs during the Phanerozoic (*28*).

We hypothesize that changes in remineralization of organic matter strongly influenced the upper-ocean I/Ca signature (Fig. 2), and we tested this hypothesis by simulating the marine iodine cycle in the 'cGENIE' Earth system model (see Methods, fig. S5) (*29*). We aimed to identify possible causes for low I/Ca during the Paleozoic through ensembles of model runs using a range of values for atmospheric pO_2, the depth of organic-matter remineralization in the water column, and the mean concentrations of iodine and phosphate in seawater. For each Paleozoic model run, surface-water [IO_3^-] values along continental margins were extracted to calculate a relative frequency distribution (fig. S6). The modeled IO_3^- distributions were compared with observed Paleozoic I/Ca distributions (Fig. 1C) to obtain the residual sum of squares (RSS) (see Materials and Methods, Fig. 4A and fig. S7).

We found that the lowest RSS values (<0.05), representing the best data-model fits, were achieved at shallow remineralization depths [i.e., <0.5 present oceanic level (POL)]. In the same set of cGENIE runs (Fig. 4B), lower RSS values correlated with lower average [O_2] in the subsurface layer (80-176 m), which is consistent with a shallower oxycline. Even as Paleozoic oceans experienced transitions between greenhouse and icehouse climate conditions, pCO_2 levels appear to have had minimal influence on IO_3^- distributions (fig. S8). Global-scale changes in ocean circulation and continent configuration also do not significantly influence the oxycline depths independently of pO_2 and subsurface oxygen consumption (fig. S9). The RSS contours differed only slightly when the Paleozoic I/Ca distribution was compared with modeled [IO_3^-] distributions in the top four layers in the upper ocean (from 0 to 410 m, fig. S10). Thus, a lack of precise constraints on the paleo-depths of carbonate formation is unlikely to have affected the main conclusions of our data–model comparison. Additional model runs also suggest that oceanic nutrient levels and total iodine concentrations are unlikely to dominate the secular trends in proxy data (figs. S11 and S12). Our data-model comparison (Fig. 4A) should not be viewed as a precise estimate of the atmospheric pO_2 for any single time slice, since the data were compiled over the entire Paleozoic under varying pO_2 levels. Thus, the lower RSS values at pO_2 below 1 PAL suggest that some portions of the Paleozoic may have had pO_2 levels lower than today (*5*, *23*).

Based on our data compilation and model analyses, we attribute the transition at ~200 Ma from Proterozoic-like low I/Ca values in the Paleozoic (except for the mid-Devonian) to modern-like high values in the Meso-Cenozoic, to a profound increase in the average remineralization depth of organic matter in the water column. The timing of this transition is consistent with the proliferation of eukaryotic phyto- and zooplankton after the Permian-Triassic extinction (Fig. 3A) (*30*, *31*), which eventually shaped the ecological landscape of the modern ocean (*32*). The larger size of primary producers (*33*), grazing/repackaging of organic matter into fecal pellets (*34*), and/or the advent of mineralized plankton (*32*) may have led to faster sinking of organic matter, which reduced O_2 utilization in the upper water column and caused a pervasive deepening of the oxycline (*28*).

The rise of oxygen levels over geological time has been linked to increases in animal body size (*24*, *35*). A comprehensive compilation of Phanerozoic marine animal body-size data (*36*) shows that maximum bio-volume probably co-varied with I/Ca to some extent (Fig. 3B), indicating that O_2 availability in the global upper ocean may have been an important factor in Phanerozoic metazoan evolution. New forms of organisms (e.g., mineralized plankton, larger animals) fundamentally influenced oceanic environments, which in turn affected the evolving biosphere, representing a prime example of the co-evolution of life and planet.

REFERENCES AND NOTES

1. A. H. Knoll, Paleobiological perspectives on early eukaryotic evolution. *Cold Spring Harb. Perspect. Biol.* **6**, a016121 (2014). doi:10.1101/cshperspect.a016121 Medline
2. R. E. Keeling, A. Körtzinger, N. Gruber, Ocean deoxygenation in a warming world. *Ann. Rev. Mar. Sci.* **2**, 199–229 (2010). doi:10.1146/annurev.marine.010908.163855 Medline
3. T. W. Lyons, C. T. Reinhard, N. J. Planavsky, The rise of oxygen in Earth's early ocean and atmosphere. *Nature* **506**, 307–315 (2014). doi:10.1038/nature13068 Medline
4. T. W. Dahl, E. U. Hammarlund, A. D. Anbar, D. P. G. Bond, B. C. Gill, G. W. Gordon, A. H. Knoll, A. T. Nielsen, N. H. Schovsbo, D. E. Canfield, Devonian rise in atmospheric oxygen correlated to the radiations of terrestrial plants and large predatory fish. *Proc. Natl. Acad. Sci. U.S.A.* **107**, 17911–17915 (2010). doi:10.1073/pnas.1011287107 Medline
5. E. A. Sperling, C. J. Wolock, A. S. Morgan, B. C. Gill, M. Kunzmann, G. P. Halverson, F. A. Macdonald, A. H. Knoll, D. T. Johnston, Statistical analysis of iron geochemical data suggests limited late Proterozoic oxygenation. *Nature* **523**, 451–454 (2015). doi:10.1038/nature14589 Medline
6. Z. Lu, B. A. A. Hoogakker, C.-D. Hillenbrand, X. Zhou, E. Thomas, K. M. Gutchess, W. Lu, L. Jones, R. E. M. Rickaby, Oxygen depletion recorded in upper waters of the glacial Southern Ocean. *Nat. Commun.* **7**, 11146 (2016). doi:10.1038/ncomms11146 Medline
7. Z. Lu, H. C. Jenkyns, R. E. M. Rickaby, Iodine to calcium ratios in marine carbonate as a paleo-redox proxy during oceanic anoxic events. *Geology* **38**, 1107–1110 (2010). doi:10.1130/G31145.1
8. G. W. Luther III, T. Campbell, Iodine speciation in the water column of the Black Sea. *Deep-Sea Res. A, Oceanogr. Res. Pap.* **38**, S875–S882 (1991). doi:10.1016/S0198-0149(10)80014-7
9. E. L. Rue, G. J. Smith, G. A. Cutter, K. W. Bruland, The response of trace element redox couples to suboxic conditions in the water column. *Deep Sea Res. Part I Oceanogr. Res. Pap.* **44**, 113–134 (1997). doi:10.1016/S0967-0637(96)00088-X
10. J. Podder, J. Lin, W. Sun, S. M. Botis, J. Tse, N. Chen, Y. Hu, D. Li, J. Seaman, Y.

Pan, Iodate in calcite and vaterite: Insights from synchrotron x-ray absorption spectroscopy and first-principles calculations. *Geochim. Cosmochim. Acta* **198**, 218–228 (2017). doi:10.1016/j.gca.2016.11.032
11. D. S. Hardisty, Z. Lu, A. Bekker, C. W. Diamond, B. C. Gill, G. Jiang, L. C. Kah, A. H. Knoll, S. J. Loyd, M. R. Osburn, N. J. Planavsky, C. Wang, X. Zhou, T. W. Lyons, Perspectives on Proterozoic surface ocean redox from iodine contents in ancient and recent carbonate. *Earth Planet. Sci. Lett.* **463**, 159–170 (2017). doi:10.1016/j.epsl.2017.01.032
12. D. S. Hardisty, Z. Lu, N. J. Planavsky, A. Bekker, P. Philippot, X. Zhou, T. W. Lyons, An iodine record of Paleoproterozoic surface ocean oxygenation. *Geology* **42**, 619–622 (2014). doi:10.1130/G35439.1
13. X. Zhou, H. C. Jenkyns, J. D. Owens, C. K. Junium, X.-Y. Zheng, B. B. Sageman, D. S. Hardisty, T. W. Lyons, A. Ridgwell, Z. Lu, Upper ocean oxygenation dynamics from I/Ca ratios during the Cenomanian-Turonian OAE 2. *Paleoceanography* **30**, 510–526 (2015). doi:10.1002/2014PA002741
14. X. L. Zhou, E. Thomas, R. E. M. Rickaby, A. M. E. Winguth, Z. L. Lu, I/Ca evidence for upper ocean deoxygenation during the PETM. *Paleoceanography* **29**, 964–975 (2014). doi:10.1002/2014PA002702
15. W. Lu, S. Wörndle, G. P. Halverson, X. Zhou, A. Bekker, R. H. Rainbird, D. S. Hardisty, T. W. Lyons, Z. Lu, Iodine proxy evidence for increased ocean oxygenation during the Bitter Springs Anomaly. *Geochem. Perspect. Lett.* **5**, 53–57 (2017). doi:10.7185/geochemlet.1746
16. C. T. Edwards, D. A. Fike, M. R. Saltzman, W. Lu, Z. Lu, Evidence for local and global redox conditions at an Early Ordovician (Tremadocian) mass extinction. *Earth Planet. Sci. Lett.* **481**, 125–135 (2018). doi:10.1016/j.epsl.2017.10.002
17. G. R. Loope, L. R. Kump, M. A. Arthur, Shallow water redox conditions from the Permian–Triassic boundary microbialite: The rare earth element and iodine geochemistry of carbonates from Turkey and South China. *Chem. Geol.* **351**, 195–208 (2013). doi:10.1016/j.chemgeo.2013.05.014
18. R. Chance, A. R. Baker, L. Carpenter, T. D. Jickells, The distribution of iodide at the sea surface. *Environ. Sci. Process. Impacts* **16**, 1841–1859 (2014). doi:10.1039/C4EM00139G Medline
19. T. M. Lenton, T. W. Dahl, S. J. Daines, B. J. W. Mills, K. Ozaki, M. R. Saltzman, P. Porada, Earliest land plants created modern levels of atmospheric oxygen. *Proc. Natl. Acad. Sci. U.S.A.* **113**, 9704–9709 (2016). doi:10.1073/pnas.1604787113 Medline
20. I. J. Glasspool, A. C. Scott, Phanerozoic concentrations of atmospheric oxygen reconstructed from sedimentary charcoal. *Nat. Geosci.* **3**, 627–630 (2010). doi:10.1038/ngeo923
21. R. A. Berner, GEOCARBSULF: A combined model for Phanerozoic atmospheric O_2 and CO_2. *Geochim. Cosmochim. Acta* **70**, 5653–5664 (2006). doi:10.1016/j.gca.2005.11.032
22. N. M. Bergman, T. M. Lenton, A. J. Watson, COPSE: A new model of biogeochemical cycling over Phanerozoic time. *Am. J. Sci.* **304**, 397–437 (2004). doi:10.2475/ajs.304.5.397
23. T. M. Lenton, S. J. Daines, B. J. Mills, COPSE reloaded: An improved model of biogeochemical cycling over Phanerozoic time. *Earth Sci. Rev.* **178**, 1–28 (2018). doi:10.1016/j.earscirev.2017.12.004
24. P. G. Falkowski, M. E. Katz, A. J. Milligan, K. Fennel, B. S. Cramer, M. P. Aubry, R. A. Berner, M. J. Novacek, W. M. Zapol, The rise of oxygen over the past 205 million years and the evolution of large placental mammals. *Science* **309**, 2202–2204 (2005). doi:10.1126/science.1116047 Medline
25. L. R. Kump, Terrestrial feedback in atmospheric oxygen regulation by fire and phosphorus. *Nature* **335**, 152–154 (1988). doi:10.1038/335152a0
26. T. J. Algeo, R. A. Berner, J. B. Maynard, S. E. Scheckler, Late Devonian oceanic anoxic events and biotic crises: "Rooted" in the evolution of vascular land plants? *GSA Today* **5**, 64–66 (1995).
27. H. D. Holland, The oxygenation of the atmosphere and oceans. *Philos. Trans. R. Soc. Lond. B Biol. Sci.* **361**, 903–915 (2006). doi:10.1098/rstb.2006.1838 Medline
28. K. M. Meyer, A. Ridgwell, J. L. Payne, The influence of the biological pump on ocean chemistry: Implications for long-term trends in marine redox chemistry, the global carbon cycle, and marine animal ecosystems. *Geobiology* **14**, 207–219 (2016). doi:10.1111/gbi.12176 Medline
29. A. Ridgwell, J. C. Hargreaves, N. R. Edwards, J. D. Annan, T. M. Lenton, R. Marsh, A. Yool, A. Watson, Marine geochemical data assimilation in an efficient Earth System Model of global biogeochemical cycling. *Biogeosciences* **4**, 87–104 (2007). doi:10.5194/bg-4-87-2007
30. M. E. Katz, Z. V. Finkel, D. Grzebyk, A. H. Knoll, P. G. Falkowski, Evolutionary trajectories and biogeochemical impacts of marine eukaryotic phytoplankton. *Annu. Rev. Ecol. Evol. Syst.* **35**, 523–556 (2004). doi:10.1146/annurev.ecolsys.35.112202.130137
31. R. E. Martin, Cyclic and secular variation in microfossil biomineralization: Clues to the biogeochemical evolution of Phanerozoic oceans. *Global Planet. Change* **11**, 1–23 (1995). doi:10.1016/0921-8181(94)00011-2
32. P. G. Falkowski, M. E. Katz, A. H. Knoll, A. Quigg, J. A. Raven, O. Schofield, F. J. Taylor, The evolution of modern eukaryotic phytoplankton. *Science* **305**, 354–360 (2004). doi:10.1126/science.1095964 Medline
33. N. J. Butterfield, Oxygen, animals and oceanic ventilation: An alternative view. *Geobiology* **7**, 1–7 (2009). doi:10.1111/j.1472-4669.2009.00188.x Medline
34. G. A. Logan, J. M. Hayes, G. B. Hieshima, R. E. Summons, Terminal Proterozoic reorganization of biogeochemical cycles. *Nature* **376**, 53–56 (1995). doi:10.1038/376053a0 Medline
35. J. L. Payne, C. R. McClain, A. G. Boyer, J. H. Brown, S. Finnegan, M. Kowalewski, R. A. Krause Jr., S. K. Lyons, D. W. McShea, P. M. Novack-Gottshall, F. A. Smith, P. Spaeth, J. A. Stempien, S. C. Wang, The evolutionary consequences of oxygenic photosynthesis: A body size perspective. *Photosynth. Res.* **107**, 37–57 (2011). doi:10.1007/s11120-010-9593-1 Medline
36. N. A. Heim, M. L. Knope, E. K. Schaal, S. C. Wang, J. L. Payne, Cope's rule in the evolution of marine animals. *Science* **347**, 867–870 (2015). doi:10.1126/science.1260065 Medline
37. L. Cao, M. Eby, A. Ridgwell, K. Caldeira, D. Archer, A. Ishida, F. Joos, K. Matsumoto, U. Mikolajewicz, A. Mouchet, J. C. Orr, G.-K. Plattner, R. Schlitzer, K. Tokos, I. Totterdell, T. Tschumi, Y. Yamanaka, A. Yool, The role of ocean transport in the uptake of anthropogenic CO_2. *Biogeosciences* **6**, 375–390 (2009). doi:10.5194/bg-6-375-2009
38. A. Tagliabue, O. Aumont, R. DeAth, J. P. Dunne, S. Dutkiewicz, E. Galbraith, K. Misumi, J. K. Moore, A. Ridgwell, E. Sherman, C. Stock, M. Vichi, C. Völker, A. Yool, How well do global ocean biogeochemistry models simulate dissolved iron distributions? *Global Biogeochem. Cycles* **30**, 149–174 (2016). doi:10.1002/2015GB005289
39. H. Elderfield, V. W. Truesdale, On the biophilic nature of iodine in seawater. *Earth Planet. Sci. Lett.* **50**, 105–114 (1980). doi:10.1016/0012-821X(80)90122-3
40. S. K. Lyons, K. L. Amatangelo, A. K. Behrensmeyer, A. Bercovici, J. L. Blois, M. Davis, W. A. DiMichele, A. Du, J. T. Eronen, J. T. Faith, G. R. Graves, N. Jud, C. Labandeira, C. V. Looy, B. McGill, J. H. Miller, D. Patterson, S. Pineda-Munoz, R. Potts, B. Riddle, R. Terry, A. Tóth, W. Ulrich, A. Villaseñor, S. Wing, H. Anderson, J. Anderson, D. Waller, N. J. Gotelli, Holocene shifts in the assembly of plant and animal communities implicate human impacts. *Nature* **529**, 80–83 (2016). doi:10.1038/nature16447 Medline
41. L. A. Hardie, Secular variations in Precambrian seawater chemistry and the timing of Precambrian aragonite seas and calcite seas. *Geology* **31**, 785–788 (2003). doi:10.1130/G19657.1
42. J. Farkaš, F. Böhm, K. Wallmann, J. Blenkinsop, A. Eisenhauer, R. van Geldern, A. Munnecke, S. Voigt, J. Veizer, Calcium isotope record of Phanerozoic oceans: Implications for chemical evolution of seawater and its causative mechanisms. *Geochim. Cosmochim. Acta* **71**, 5117–5134 (2007). doi:10.1016/j.gca.2007.09.004
43. A. Ridgwell, A Mid Mesozoic Revolution in the regulation of ocean chemistry. *Mar. Geol.* **217**, 339–357 (2005). doi:10.1016/j.margeo.2004.10.036
44. T. K. Lowenstein, L. A. Hardie, M. N. Timofeeff, R. V. Demicco, Secular variation in seawater chemistry and the origin of calcium chloride basinal brines. *Geology* **31**, 857–860 (2003). doi:10.1130/G19728R.1
45. R. A. Berner, A model for calcium, magnesium and sulfate in seawater over Phanerozoic time. *Am. J. Sci.* **304**, 438–453 (2004). doi:10.2475/ajs.304.5.438
46. L. A. Hardie, Secular variation in seawater chemistry: An explanation for the coupled secular variation in the mineralogies of marine limestones and potash evaporites over the past 600 m.y. *Geology* **24**, 279–283 (1996). doi:10.1130/0091-7613(1996)024<0279:SVISCA>2.3.CO;2
47. A. Ridgwell, D. N. Schmidt, Past constraints on the vulnerability of marine calcifiers to massive carbon dioxide release. *Nat. Geosci.* **3**, 196–200 (2010).

doi:10.1038/ngeo755
48. A. Schmidt, R. A. Skeffington, T. Thordarson, S. Self, P. M. Forster, A. Rap, A. Ridgwell, D. Fowler, M. Wilson, G. W. Mann, P. B. Wignall, K. S. Carslaw, Selective environmental stress from sulphur emitted by continental flood basalt eruptions. *Nat. Geosci.* **9**, 77–82 (2016). doi:10.1038/ngeo2588
49. F. M. Monteiro, R. D. Pancost, A. Ridgwell, Y. Donnadieu, Nutrients as the dominant control on the spread of anoxia and euxinia across the Cenomanian-Turonian oceanic anoxic event (OAE2): Model-data comparison. *Paleoceanography* **27**, PA4209 (2012). doi:10.1029/2012PA002351
50. B. Kendall, T. Komiya, T. W. Lyons, S. M. Bates, G. W. Gordon, S. J. Romaniello, G. Jiang, R. A. Creaser, S. Xiao, K. McFadden, Y. Sawaki, M. Tahata, D. Shu, J. Han, Y. Li, X. Chu, A. D. Anbar, Uranium and molybdenum isotope evidence for an episode of widespread ocean oxygenation during the late Ediacaran Period. *Geochim. Cosmochim. Acta* **156**, 173–193 (2015). doi:10.1016/j.gca.2015.02.025
51. X. Zhou, H. C. Jenkyns, W. Lu, D. S. Hardisty, J. D. Owens, T. W. Lyons, Z. Lu, Organically bound iodine as a bottom-water redox proxy: Preliminary validation and application. *Chem. Geol.* **457**, 95–106 (2017). doi:10.1016/j.chemgeo.2017.03.016

ACKNOWLEDGMENTS

Funding: We thank NSF EAR-1349252, OCE-1232620, OCE-1736542 (Z.L.); NERC NE/J01043X/1, ERC-2013-CoG-617313, NSF OCE-1736771 (A.R.); NSF OCE-1736538 (E.T.); National Key R&D Project of China (2016YFA0601104) and NSFC 41290260 (G.L.); CAS (QYZDY-SSW-DQC031) and the "111" project (Y.S.); Wolfson Research Merit award from the Royal Society and EU award (R.E.M.R.); NERC NE/N018508/1, NE/P013643/1 (T.M.L.). **Author contributions:** Z.L. conceived the study. W.L. and Z.L. carried out the data analysis, model simulations and wrote the paper. A.R. modified cGENIE to incorporate iodine cycle. All authors contributed to data interpretation and the writing of the manuscript. **Competing interests:** The authors declare that they have no competing interests. **Data and materials availability:** all I/Ca data are available in the supplementary materials and online from https://www.pangaea.de/.

SUPPLEMENTARY MATERIALS

www.sciencemag.org/cgi/content/full/science.aar5372/DC1
Materials and Methods
Figs. S1 to S12
References (*37*–*51*)
Tables S1 and S2

20 November 2017; accepted 17 May 2018
Published online 31 May 2018
10.1126/science.aar5372

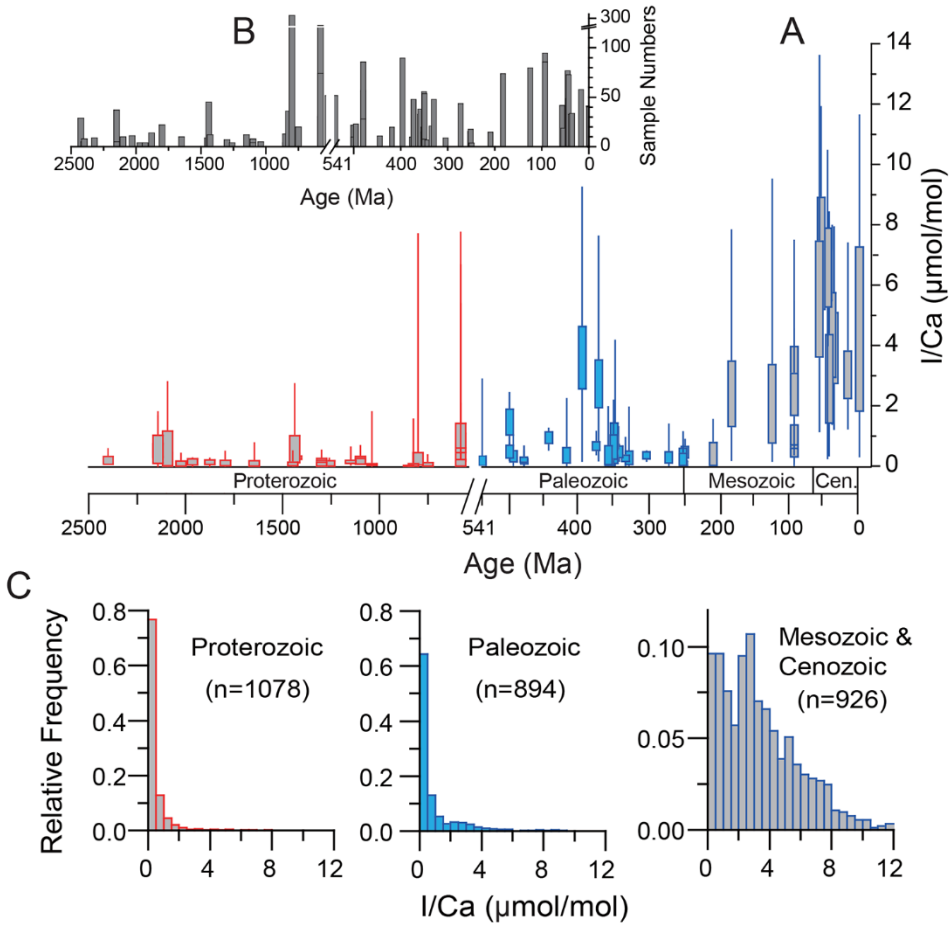

Fig. 1. Carbonate I/Ca through time. (**A**) Candlestick plot showing ranges of I/Ca values for Proterozoic (red) (*11*, *15*), Paleozoic (blue) and Meso-Cenozoic (purple). Boxes mark the 25th and 75th percentiles of values at each locality, and the whiskers show the maximum and minimum. Note that the Proterozoic values from dolostones are I/(Mg+Ca). (**B**) Number of samples measured at each section. (**C**) Relative frequency distributions of I/Ca.

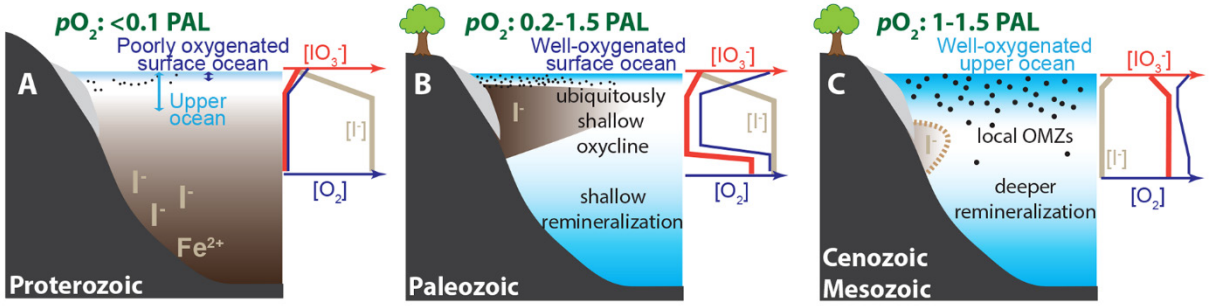

Fig. 2. Schematic illustrations for the evolution of oxygenation conditions. These simplified cartoons are not intended to capture all temporal and spatial variations.

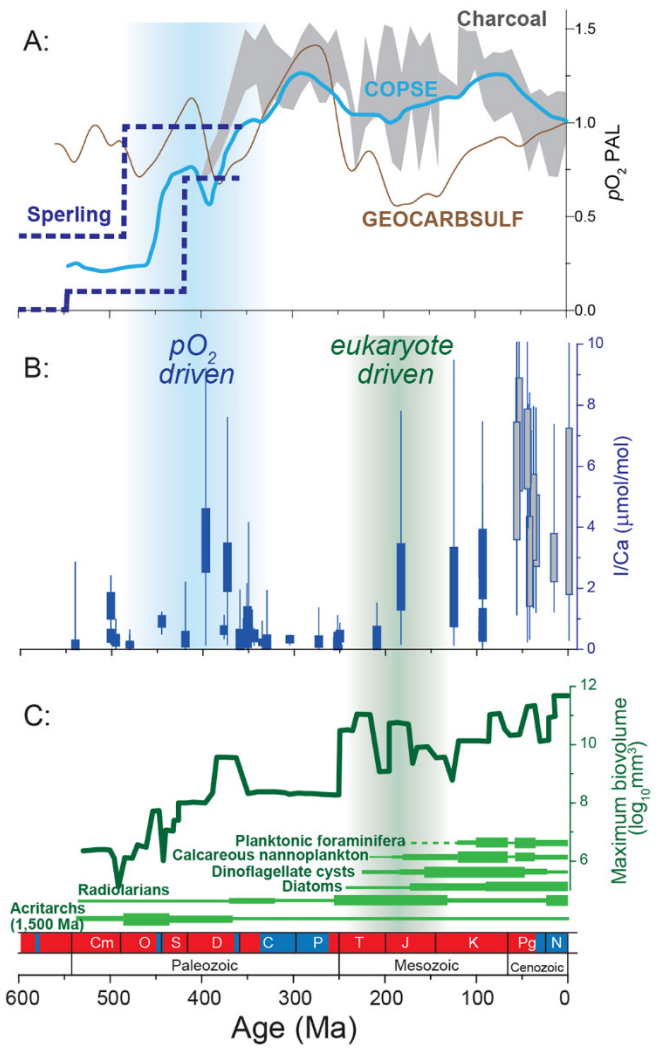

Fig. 3. Phanerozoic I/Ca compared with atmospheric pO_2, oceanic oxygenation and animal evolution trends. (**A**) Modeled atmospheric pO_2 curves (*5*, *21*, *23*, *24*) in comparison with the charcoal proxy record (*20*). Dashed lines (*5*) mark a broadly defined ocean-atmospheric O_2 level, not just atmospheric pO_2. (**B**) I/Ca records through Phanerozoic. Blue boxes for bulk carbonate rock, gray boxes for bulk coarse fraction of Ocean Drilling Project samples (>63 µm). (**C**) Marine animal body size record (*36*). Thickness of green bars indicates relative generic diversity modified from literature (*31*, *32*). The red *vs* blue bars mark greenhouse *vs* icehouse climate conditions, respectively.

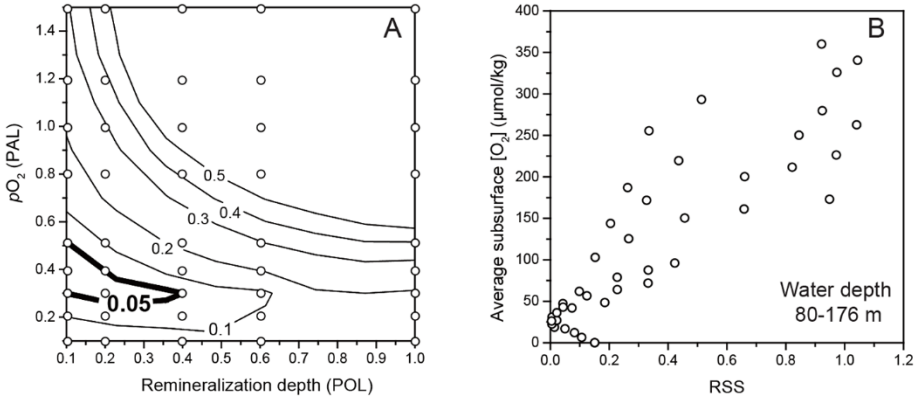

Fig. 4. Residual sum of squares (RSS) and subsurface $[O_2]$ at different pO_2 levels and remineralization depths. (**A**) Shallow remineralization depths (POL for present oceanic level) produce the best model fit (the smallest RSS < 0.05) to Paleozoic I/Ca distribution, at 1× CO_2 condition. White dots represent 45 cGENIE simulations defining the contours. (**B**) Averaged $[O_2]$ in the shallowest subsurface layer in each cGENIE run as an indicator of oxycline depth correlating with the RSS.

Science

Late inception of a resiliently oxygenated upper ocean

Wanyi Lu, Andy Ridgwell, Ellen Thomas, Dalton S. Hardisty, Genming Luo, Thomas J. Algeo, Matthew R. Saltzman, Benjamin C. Gill, Yanan Shen, Hong-Fei Ling, Cole T. Edwards, Michael T. Whalen, Xiaoli Zhou, Kristina M. Gutchess, Li Jin, Rosalind E. M. Rickaby, Hugh C. Jenkyns, Timothy W. Lyons, Timothy M. Lenton, Lee R. Kump and Zunli Lu

published online May 31, 2018

Science (print ISSN 0036-8075; online ISSN 1095-9203) is published by the American Association for the Advancement of Science, 1200 New York Avenue NW, Washington, DC 20005.